Integrated Waveform Design of Radar and Communication Based on Chirp-rate Hopping Modulation

*Guoqi ZHANG, Xuan RAO, Jilin FU, Wenwen HU, Jianfen HU**

Nanchang Hangkong University, Nanchang 330063, China

*ffeenn777@163.com

Submitted October 17, 2024 / Accepted December 27, 2024 / Online first March 10, 2025

Abstract. *The increasing demand for spectrum resources and the need for reducing the burden of modern electronic combat platforms have prompted the development of integrated radar and communication systems. An integrated radar and communication waveform scheme based on Chirp-rate Hopping Modulation (CrHM) is proposed in this paper to realize target detection and information transmission simultaneously. The CrHM signal can be regarded as the synthesis of multiple sub-pulses, and each sub-pulse is a Chirp signal, which is determined by the communication information sequence. The performance of the CrHM signal is analyzed, including the ambiguity function, the principle of demodulation, and the robust properties of demodulation. Subsequently, several simulations are provided to testify the high weak target detection performance of the CrHM signal and robustness of demodulation.*

Keywords

Integrated radar and communication, waveform design, chirp-rate, chirp-rate hopping modulation, weak target detection

1. Introduction

With the rapid development of electronic and information technology, spectrum resources are increasingly scarce, and the loading of various equipment, such as radar and communication equipment, is required by modern information warfare on a same combat platform [1–5]. Although the superposition of various equipment has improved the combat capability, it faces the problems of large power consumption and volume, and serious electromagnetic interference. Therefore, it is important to reduce the burden of the platform by integrating the design of radar and communication [6–8].

Current research on integrated waveform of radar and communication can be divided into two categories, namely coexistence and shared system [9–12]. In the coexistence system, radar and communication occupy different resources in the time domain [13], frequency domain [14] and spatial domain [15], [16], etc. However, the major problems of coexistence system are poor real-time performance and low spectrum utilization in radar detection and wireless communication. Nevertheless, for the shared system, radar detection and wireless communication functions are realized simultaneously through a single waveform, which can effectively overcome the problem of coexistence system.

Linear frequency modulation (LFM) signal is widely used because of its large time-bandwidth product. In [17], the communication modulation method of minimum shift keying (MSK) is studied to embed the communication information into the LFM pulse, but the communication rate of this scheme is not high enough. To improve the communication rate, high-order quadrature amplitude modulation (QAM) has been involved in [18] and [19], which cannot maintain a constant envelope due to the modulation for the amplitude and phase of the waveform, and an increase in the modulation order will lead to a decline in the performance of bit error rate (BER). In [20], the integrated waveform of radar and communication is designed by using a frequency modulation (FM) scheme with orthogonal FM function [21] to transmit communication information, which operates on the phase term to ensure the constant envelope characteristic. In [22], a waveform design method using staggered pulse repetition frequency (PRF) is proposed, which improves the Doppler tolerance and the detection efficiency, and solves the common problem of Doppler sensitivity effectively in radar detection of moving target.

Based on the characteristic that the Fractional Fourier Transform (FRFT) has excellent energy aggregation for chirp signals, an integrated radar and communication waveform based on Chirp-rate Hopping Modulation (CrHM) is proposed in this paper, which is a shared waveform with constant envelope and some Doppler tolerance. The constant envelope makes it satisfy the requirement that the power amplifier of modern radar works in the saturated

DOI: 10.13164/re.2025.0028

state, and the Doppler tolerance solves the problem of Doppler sensitivity in the radar detection of moving target and improves the detection performance. The rest of the paper is organized as follows: The integrated waveform based on CrHM is proposed and the integrated system scheme is given in Sec. 2. The performance of the proposed waveform is analyzed in Sec. 3. The accuracy of the theoretical analysis is verified by numerical simulation in Sec. 4. Finally, the conclusion is given in Sec. 5.

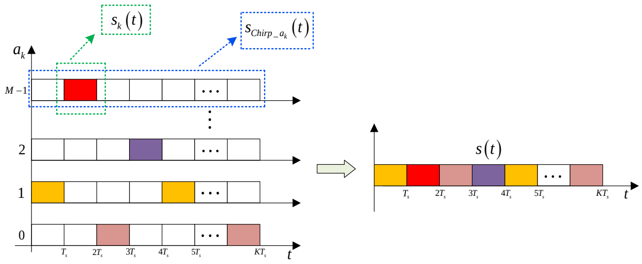

Fig. 1. CrHM signal synthesis process.

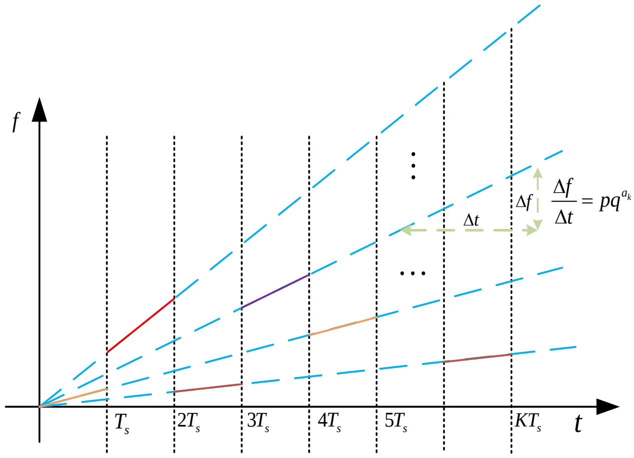

Fig. 2. Time-frequency relationship of CrHM signal.

2. Integrated Waveform Design Based on Chirp-rate Hopping Modulation

Assuming that each pulse of the CrHM signal contains K sub-pulses, each of which is a chirp signal. The communication symbol determines the chirp-rate of chirp pulse signal, and the position of the symbol in the transmitted communication sequence determines the sub-pulse position of the chirp signal corresponding to the symbol. The synthesis process of the integrated waveform is shown in Fig. 1 and the time-frequency diagram of CrHM signal is given in Fig. 2.

Consider the chirp signal corresponding to the communication symbol a_k as

$$s_{\mathrm{Chirp}\_a_k}(t) = \mathrm{rect}\left(\frac{t}{T_p}\right)\exp\left(\mathrm{j}\pi p q^{a_k} t^2\right) \tag{1}$$

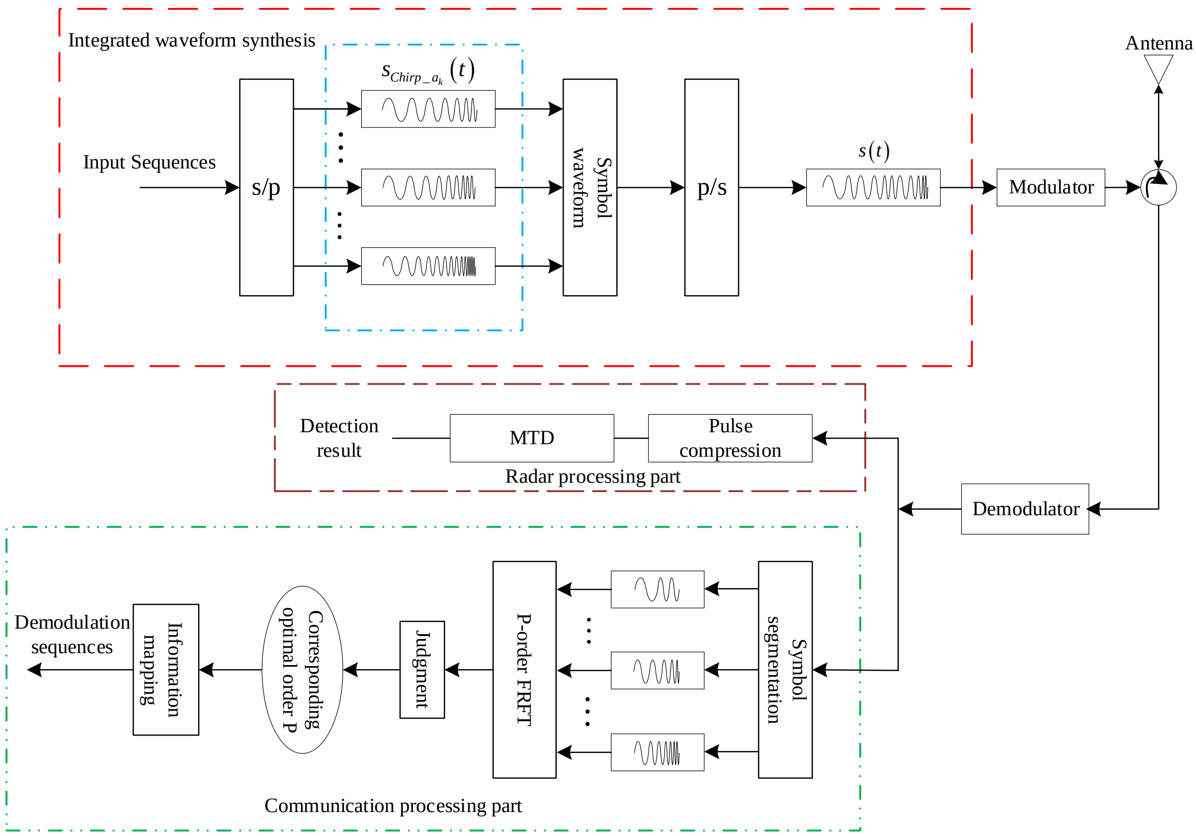

Fig. 3. Integrated radar and communication system architecture based on CrHM.

where $\operatorname{rect}\left(\frac{t}{T_p}\right)=\begin{cases}1, & 0\le t\le T_p\\ 0, & \text{else}\end{cases}$, ; $T_p = \mathrm{k}T_s$ is the pulse duration, T_s represents the symbol duration, K is the number of transmitted communication symbols; $a_k \in \{0,1,\ldots,M-1\}$, and it represents the communication information of M-ary modulation, $k = 0,1,\ldots,K-1$; p, q together with the communication information sequences form the chirp-rate.

$s_{\mathrm{Chirp}\_a_k}(t)$ is divided into K sub-pulses according to the symbol width. If the symbol a_k is the k-th symbol in the transmitted communication sequence, then the symbol waveform can be expressed as

$$s_k(t)=\operatorname{rect}\left(\frac{t-kT_\mathrm{s}}{T_\mathrm{s}}\right)s_{\mathrm{Chirp}\_a_k}(t). \tag{2}$$

Finally, the baseband expression of the CrHM signal can be written as

$$s(t)=\sum_{k=0}^{K-1}s_k(t). \tag{3}$$

The proposed integrated radar and communication system architecture based on CrHM is shown in Fig. 3, which is mainly divided into three parts, namely, integrated waveform synthesis, radar processing and communication processing. The corresponding chirp signal is generated after the serial-parallel (s/p) conversion of the input communication information sequences, and then the symbol waveform is obtained according to the position of the communication information. Finally, these symbol waveforms are synthesized into the integrated waveform after the parallel-serial (p/s) conversion. For target detection, the pulse compression technique and the moving target detection (MTD) within a coherent processing time (CPT) are used to raise the signal-to-noise ratio (SNR) to improve the radar detection performance. Meanwhile, the communication receiver receives the integrated signal and demodulates the communication information.

3. Waveform Performance Analysis

3.1 Ambiguity Function of the Proposed Waveform

To show the radar performance of the proposed waveform, the radar ambiguity function expression is given in this section. The ambiguity function of the CrHM signal can be defined as

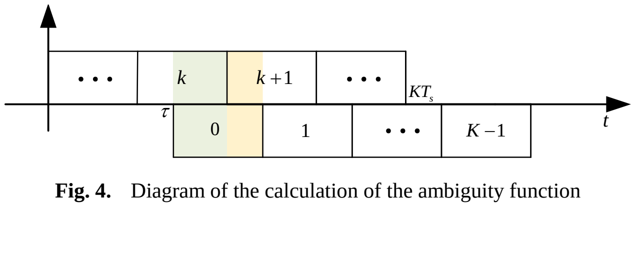

Fig. 4. Diagram of the calculation of the ambiguity function

$$\begin{aligned}\chi(\tau, f_\mathrm{d}) &= \int_{-\infty}^{+\infty} s(t)s^*(t-\tau)\,\mathrm{e}^{\mathrm{j}2\pi f_\mathrm{d}t}\,\mathrm{d}t\\ &=\int_{-\infty}^{+\infty}\sum_{k=0}^{K-1}\operatorname{rect}\left(\frac{t-kT_\mathrm{s}}{T_\mathrm{s}}\right)\exp\left(\mathrm{j}\pi pq^{a_k}t^2\right)\\ &\quad\times\sum_{l=0}^{K-1}\operatorname{rect}\left(\frac{t-\tau-lT_\mathrm{s}}{T_\mathrm{s}}\right)\exp\left(-\mathrm{j}\pi pq^{a_l}(t-\tau)^2\right)\\ &\quad\times\exp\left(\mathrm{j}2\pi f_\mathrm{d}t\right)\mathrm{d}t\end{aligned} \tag{4}$$

where τ is the time delay, f_d is the Doppler frequency, and $s^*(t)$ represents the conjugation of $s(t)$.

Since the ambiguity function has the characteristic of symmetry about the origin, only the case that $\tau \ge 0$ is analyzed here. The calculation diagram of the ambiguity function is shown in Fig. 4.

Because the $pq^{a_k}t^2$ is in the exponential term, it is difficult to obtain the closed form expression of the ambiguity function. According to (4), $\chi(\tau, f_\mathrm{d})$ is the mainlobe χ_m when k equals l. Therefore, the χ_m is discussed in this paper, which can be expressed as

$$\begin{aligned}&\chi_m(\tau, f_\mathrm{d}) =\\ &\sum_{k=0}^{K-1}\exp\left(-\mathrm{j}\pi pq^{a_k}\tau^2\right)\int_{\tau+kT_\mathrm{s}}^{(k+1)T_\mathrm{s}}\exp\left(\mathrm{j}2\pi\left(pq^{a_k}\tau+f_\mathrm{d}\right)t\right)\mathrm{d}t\\ &=\left(T_\mathrm{s}-\tau\right)\sum_{k=0}^{K-1}\exp\left(\mathrm{j}\pi\begin{pmatrix}(2k+1)\,pq^{a_k}T_\mathrm{s}\tau+\\ \left((2k+1)T_\mathrm{s}+\tau\right)f_\mathrm{d}\end{pmatrix}\right)\\ &\times\operatorname{sinc}\left(\pi\left(pq^{a_k}\tau+f_\mathrm{d}\right)\left(T_\mathrm{s}-\tau\right)\right)\end{aligned} \tag{5}$$

Obviously, the ambiguity function of the CrHM signal is affected not only by the time delay and Doppler frequency, but also by the communication information sequences. In addition, when the transmitted communication symbol a_k is a constant value, the CrHM signal will degenerate into a single chirp signal, and the ambiguity function of the CrHM signal will degenerate into the ambiguity function of the chirp signal. On the contrary, when it is non-constant value, the ambiguity function of CrHM signal can be regarded as the composition of the ambiguity function of multiple sub-chirp signals determined by a_k. So the combination of sub-chirp signals with the same chirp-rate will make the oblique blade with a certain angle which is relative to the chirp-rate, while sub-chirp signals with different chirp-rate will partially cancel each other, so that the ambiguity function has a thumbtack shape.

Especially, when $\tau = 0$, the zero-delay cut is a sinc function, i.e.

$$\chi_m(0, f_\mathrm{d}) = T_\mathrm{s}\sum_{k=0}^{K-1}\exp\left(\mathrm{j}\pi\left((2k+1)T_\mathrm{s}f_\mathrm{d}\right)\right)\operatorname{sinc}\left(\pi f_d T_\mathrm{s}\right) \tag{6}$$

while, when $f_\mathrm{d} = 0$, the zero-Doppler cut is

$$\begin{aligned}\chi_m(\tau,0) &= \left(T_\mathrm{s}-\tau\right)\sum_{k=0}^{K-1}\exp\left(\mathrm{j}\pi(2k+1)\,pq^{a_k}T_\mathrm{s}\tau\right)\\ &\times\operatorname{sinc}\left(\pi pq^{a_k}\tau\left(T_\mathrm{s}-\tau\right)\right).\end{aligned} \tag{7}$$

It can be seen from (7) that the zero-Doppler cut is composed of the zero-Doppler cuts of multiple sub-Chirp signals with different parameters, which are decided by the communication information sequences and the number of transmitted communication symbols.

3.2 Principle of Demodulation

Based on the modulation scheme that the communication information carried by chirp-rate, it is desirable to use FRFT to complete information demodulation. For a signal $x(t)$, the corresponding FRFT is expressed as

$$X_\alpha(u) = F^P[x(t)] = \begin{cases} \sqrt{\dfrac{1-\mathrm{j}\cot\alpha}{2\pi}}\,\mathrm{e}^{\mathrm{j}\frac{u^2}{2}\cot\alpha}\displaystyle\int_{-\infty}^{+\infty} x(t)\,\mathrm{e}^{\mathrm{j}\left(\frac{t^2}{2}\cot\alpha - tu\csc\alpha\right)}\mathrm{d}t & \alpha \neq n\pi \\ x(u) & \alpha = 2n\pi \\ x(-u) & \alpha = (2n\pm 1)\pi \end{cases} \tag{8}$$

where P is the fractional order; α is the rotation angle of FRFT, and $\alpha = P\pi/2$; $F^P[\cdot]$ represents the operator symbol of FRFT.

Given that the implementation of the communication demodulation scheme in this paper is completed within the symbol width, the effect of the number of modulation symbols on the demodulation performance is analyzed. The FRFT of the k-th symbol waveform is calculated as follows

When $\alpha \neq n\pi$, the FRFT of (2) can be obtained

$$\begin{aligned} S_\alpha(u) &= \sqrt{\frac{1-\mathrm{j}\cot\alpha}{2\pi}}\exp\left(\mathrm{j}\frac{u^2}{2}\cot\alpha\right) \\ &\times\int_{-\infty}^{+\infty}\mathrm{rect}\left(\frac{t-kT_\mathrm{s}}{T_\mathrm{s}}\right)\exp\left(\mathrm{j}\pi pq^{a_k}t^2\right) \\ &\times\exp\left(\mathrm{j}\left(\frac{t^2}{2}\cot\alpha - tu\csc\alpha\right)\right)\mathrm{d}t \\ &= \sqrt{1-\mathrm{j}\cot\alpha}\,\exp\left(\mathrm{j}\pi u^2\cot\alpha\right) \\ &\times\int_{kT_s}^{(k+1)T_s}\exp\left(\mathrm{j}\pi\left(pq^{a_k}+\cot\alpha\right)t^2\right)\mathrm{d}t \end{aligned} \tag{9}$$

When $pq^{a_k} = -\cot\alpha$, equation (9) can be simplified as

$$S_\alpha(u) = T_\mathrm{s}\sqrt{1-\mathrm{j}\cot\alpha}\,\exp\left(\mathrm{j}\pi u^2\cot\alpha\right). \tag{10}$$

The peak of (10) can be calculated as

$$\left|S_\alpha(u)\right|^2 = \frac{T_\mathrm{s}^2}{\left|\sin\alpha\right|}. \tag{11}$$

In (11), it can be seen that when chirp-rate is consistent, the peak of FRFT at the optimal order is related to T_s. When $T_\mathrm{s} = T_p$, the peak of FRFT reaches the maximum,

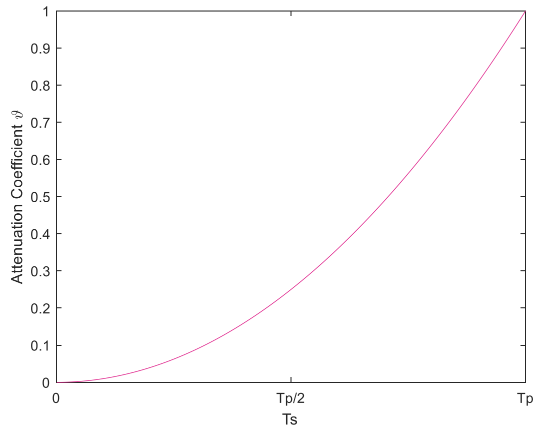

Fig. 5. Attenuation coefficient versus symbol width.

then the peak attenuation coefficient ϑ caused by T_s can be written as

$$\vartheta = \frac{T_\mathrm{s}^2}{\left|\sin\alpha\right|}\Big/\frac{T_p^2}{\left|\sin\alpha\right|} = \frac{T_\mathrm{s}^2}{T_p^2}. \tag{12}$$

Obviously, when T_p is constant, ϑ is only related to T_s, and the relationship between ϑ and T_s is shown in Fig. 5. With the increasing of T_s, i.e. the number of communication symbols transmitted within a pulse is reduced, the attenuation degree of the peak of FRFT decreases under the optimal order, which means that the BER performance of communication information demodulation is improved. Hence, the ability of a single pulse to transmit multiple bits information is limited, resulting in a low communication transfer rate.

3.3 Robust Analysis of Communication Demodulation

Since the relative motion between the radar and the target, the Doppler frequency will exist in the echoes, and the k-th symbol waveform of the echo should be

$$s_{r\_k}(t) = \mathrm{rect}\left[\frac{t-kT_\mathrm{s}}{T_\mathrm{s}}\right]\exp\left(\mathrm{j}\pi\left(pq^{a_k}t^2 + 2f_\mathrm{d}t\right)\right). \tag{13}$$

In (13), it is clear that f_d will cause the change of the center frequency, and the chirp-rate is not affected, while the change of the center frequency will cause the change of the peak position in the Fractional Fourier Domain (FRFD). Therefore, the peak offset will satisfy the following expression

$$\Delta u = f_\mathrm{d}\sin\left(\mathrm{arccot}\left(-pq^{a_k}\right)\right). \tag{14}$$

Generally, the pq^{a_k} is much larger than f_d, so the influence of Δu can be ignored. In the case of $\alpha \neq n\pi$, the FRFT of (13) is given by the following expression

$$\begin{aligned} S_\alpha(u) &= \sqrt{\frac{1-\mathrm{j}\cot\alpha}{2\pi}}\exp\left(\mathrm{j}\frac{u^2}{2}\cot\alpha\right) \\ &\times\int_{-\infty}^{+\infty}\mathrm{rect}\left(\frac{t-kT_\mathrm{s}}{T_\mathrm{s}}\right)\exp\left(\mathrm{j}\pi\left(pq^{a_k}t^2+2f_\mathrm{d}t\right)\right) \\ &\times\exp\left(\mathrm{j}\left(\frac{t^2}{2}\cot\alpha-tu\csc\alpha\right)\right)\mathrm{d}t \\ &= \sqrt{1-\mathrm{j}\cot\alpha}\exp\left(\mathrm{j}\pi u^2\cot\alpha\right) \\ &\times\int_{kT_\mathrm{s}}^{(k+1)T_\mathrm{s}}\exp\left(\mathrm{j}\pi\left(pq^{a_k}+\cot\alpha\right)t^2+\mathrm{j}2\pi f_\mathrm{d}t\right)\mathrm{d}t \end{aligned} \tag{15}$$

when $pq^{a_k}=-\cot\alpha$, equation (15) can be simplified as

$$\begin{aligned} S_\alpha(u) &= T_\mathrm{s}\sqrt{1-\mathrm{j}\cot\alpha}\exp\left(\mathrm{j}\pi u^2\cot\alpha\right) \\ &\times\exp\left(\mathrm{j}\pi f_\mathrm{d}(2k+1)T_\mathrm{s}\right)\frac{\sin(\pi f_\mathrm{d}T_\mathrm{s})}{\pi f_\mathrm{d}T_\mathrm{s}}. \end{aligned} \tag{16}$$

The peak of (16) can be calculated as

$$|S_\alpha(u)|^2 = \frac{T_\mathrm{s}^2\sin^2(\pi f_\mathrm{d}T_\mathrm{s})}{|\sin\alpha|(\pi f_\mathrm{d}T_\mathrm{s})^2}. \tag{17}$$

According to (11) and (17), the peak attenuation coefficient ρ caused by f_d is

$$\rho = \frac{T_\mathrm{s}^2\sin^2(\pi f_\mathrm{d}T_\mathrm{s})}{|\sin\alpha|(\pi f_\mathrm{d}T_\mathrm{s})^2}\Bigg/\frac{T_\mathrm{s}^2}{|\sin\alpha|} = \frac{\sin^2(\pi f_\mathrm{d}T_\mathrm{s})}{(\pi f_\mathrm{d}T_\mathrm{s})^2}. \tag{18}$$

According to the discussion given above, it can be known that ρ is only related to f_d when T_s is unchanged. Thus, the relationship between ρ and f_d can be plotted as shown in Fig. 6. It shows that when f_d reaches 2 kHz, the decrease of ρ can be neglected, so the Doppler frequency does not affect the demodulation performance of the integrated signal, which ensure the robustness of the communication demodulation.

3.4 Setting of p and q

The parameters p and q play very important roles in the CrHM signal, which together with the communication information sequences are transmitted to constitute the chirp-rate of the symbol waveform. The minimum chirp-rate interval among the communication symbols of the CrHM signal is $p(q^1-1)$. The interval ΔP of the two optimal fractional orders corresponding to the minimum chirp-rate interval determines the discrimination degree of the symbols with different chirp-rate when the FRFT is used for communication demodulation. Namely, ΔP determines the degree of interference during communication demodulation. To reduce the interference, p and q should be set to ensure ΔP is as large as possible. For the setting of p and q in the CrHM signal, it is necessary to ensure that ΔP satisfies the following expression

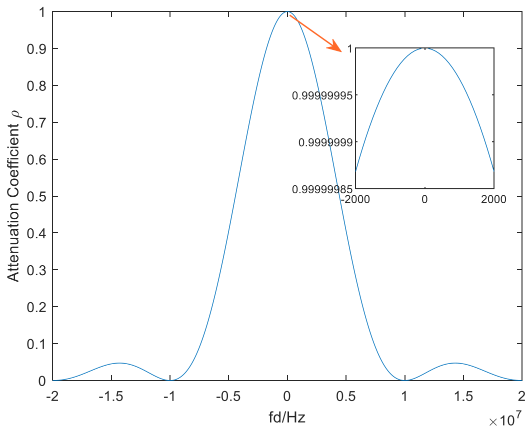

Fig. 6. Attenuation coefficient versus Doppler frequency.

$$\begin{aligned} \Delta P &= 2\left|\mathrm{arccot}\left(pq^1\right)-\mathrm{arccot}\left(pq^0\right)\right|\Big/\pi \\ &= 2\left|\mathrm{arccot}\left(pq\right)-\mathrm{arccot}\left(p\right)\right|\Big/\pi. \end{aligned} \tag{19}$$

In addition, since the time-bandwidth product of chirp signal is μT^2, chirp signal with a large chirp-rate will result in a large bandwidth for a fixed symbol width, so the values of p and q should be limited by the available bandwidth.

4. Analysis of Simulation Results

In this section, some simulation results are presented to evaluate the performance of the CrHM signal respectively. The simulation parameters of CrHM signal and the motion parameters of target are shown in Tab. 1.

4.1 Ambiguity Function

The simulation of ambiguity function is given to prove the radar performance of CrHM signal which is compared with MSK-LFM signal. The bandwidth of MSK-LFM is set to 50 MHz and each pulse of MSK-LFM transmits 16 communication symbols, which are consistent with those of CrHM signal.

The simulation results are shown in Fig. 7. It can be seen from Fig. 7(a–d) that the ambiguity function of CrHM signal is approximately composed of thumbtack shape and oblique blade shape. The CrHM signal is less sensitive to Doppler frequency than the MSK-LFM signal, therefore, it has a higher Doppler tolerance than MSK-LFM signal.

The zero-Doppler cut of CrHM signal and MSK-LFM signal is shown in Fig. 7(e). The reason why the sidelobe level of CrHM signal is higher than MSK-LFM signal that the randomness of the communication information makes the chirp-rate among different communication symbols of CrHM signal in a state of hopping. In addition, when the transmitted communication symbols are all "0" or all "1", the CrHM signal becomes a traditional LFM radar waveform.

Parameter	Value	Parameter	Value
Carrier frequency f_c	10 GHz	Number of modulation symbols K	16
Pulse repetition rate *PRF*	3 kHz	False alarm probability P_{fa}	10^{-6}
Pulse width T_p	10 µs	M-ary modulation M	2
Coherent processing time *CPT*	0.1 s	Parameter p	10^{12}
Initial distance R_0	200 km	Parameter q	5
Initial radial velocity v	100 m/s	Number of targets	1

Tab. 1. Simulation parameters of CrHM signal and the motion parameters of target.

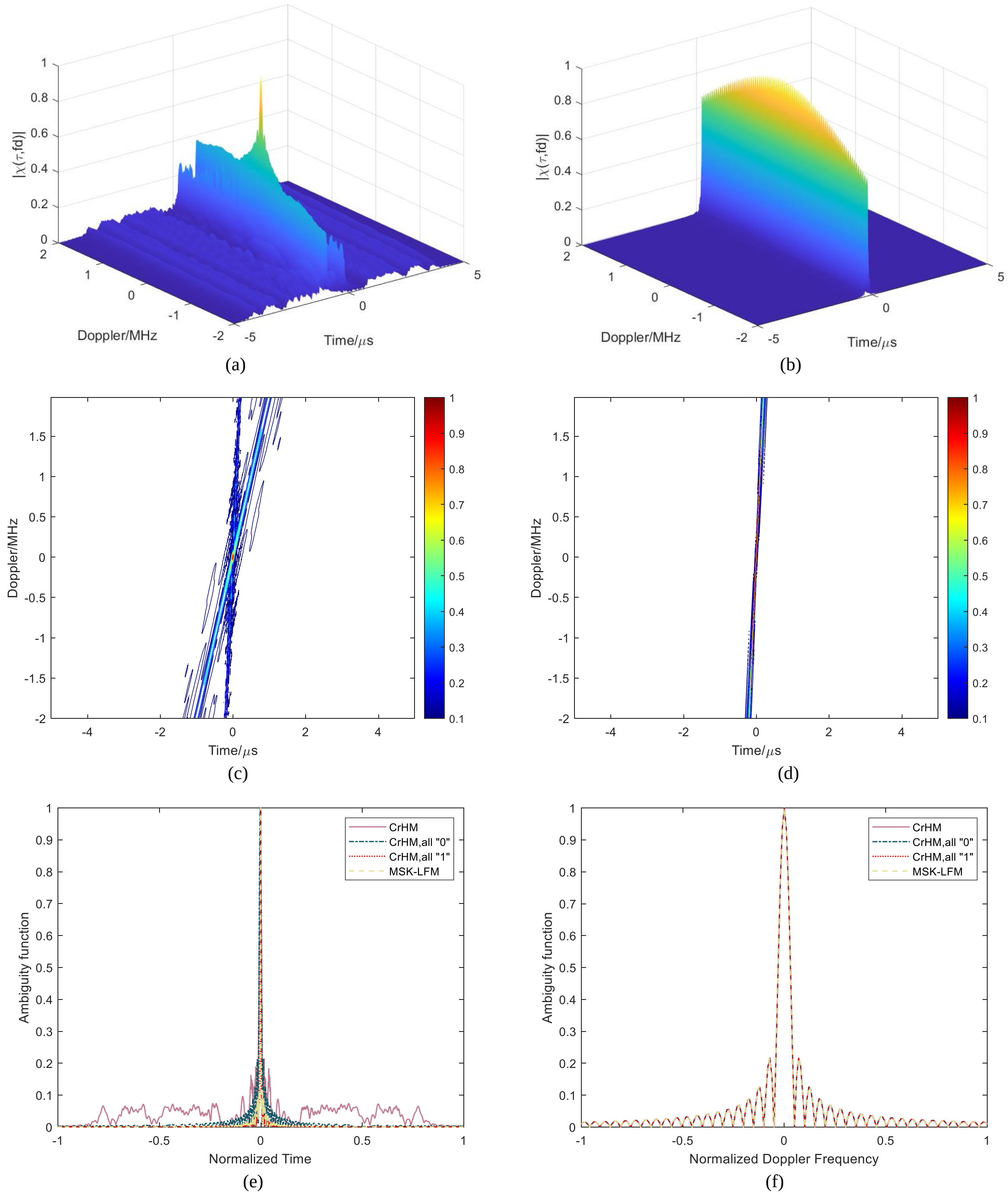

Fig. 7. Ambiguity function. (a) Ambiguity function of CrHM signal. (b) Ambiguity function of MSK-LFM signal. (c) Contour plot of CrHM signal. (d) Contour plot of MSK-LFM signal. (e) zero-Doppler cut. (f) Zero-delay cut.

Due to the randomness of the communication data, the resolution of the CrHM signal will be between the resolutions when the communication symbols are all “0” and all “1”. The zero-delay cut in Fig. 7(f) confirms that the Doppler resolution is decided by the pulse width.

4.2 Weak Target Detection

A waveform insensitive to the Doppler frequency will be more beneficial for detecting moving target. The MTD algorithm is adopted within a CPT to realize the coherent integration of the echoes. The relationship between the output of MTD and the Doppler frequency is shown in Fig. 8. It is clear that when the Doppler frequency is low, the output of MTD of the CrHM signal is equivalent to the MSK-LFM signal. However, as the Doppler frequency increases, its MTD output declines more slowly than the MSK-LFM signal, which means that the CrHM signal, which is less sensitive to Doppler frequency, is more suitable for the detection of moving target.

Finally, the comparison of detection probability is provided in Fig. 9. Obviously, the detection probability increases with the increase of SNR. When SNR = –32 dB, the detection probability of CrHM signal reaches 1; when SNR = –27 dB, the detection probability of MSK-LFM signal reaches 1. There is 5 dB improvement in detection performance between the former and the latter.

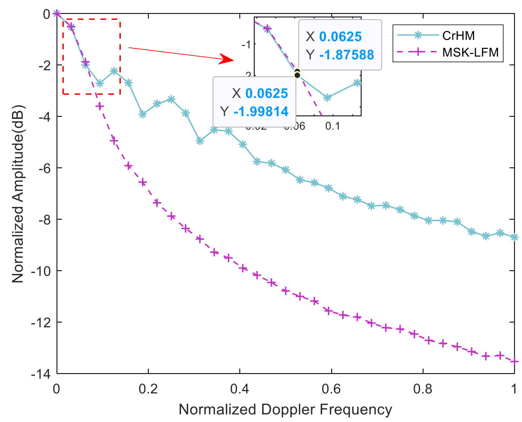

Fig. 8. Output of MTD versus Doppler frequency.

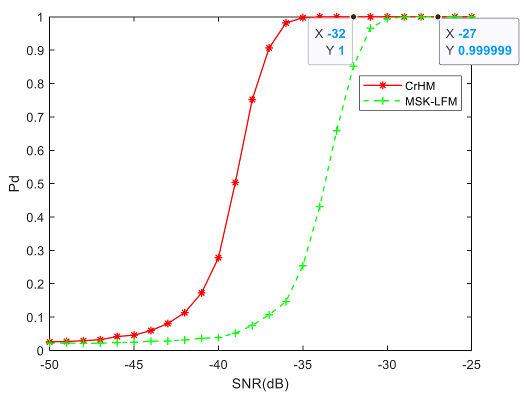

Fig. 9. Plot of detection probability.

4.3 Communication Performance

The FRFT of chirp signal will have energy aggregation at a specific order, otherwise, it does not form spectral peak, as shown in Fig. 10. The FRFT at the optimal order will have a peak, while the FRFT at other orders will not, which can achieve communication information demodulation.

The BER of different signals versus SNR is shown in Fig. 11. With the increasing of K, the BER performance of the CrHM signal decreases. In other words, the influence of symbol width on the BER performance is significant. When $K = 10$ and SNR = 9 dB, the value of BER will reach 10^{-5}, and its performance is nearly 4 dB higher than the theoretical BER performance of MSK, and obviously better than the theoretical BER performance of 2ASK and 16QAM. Another index of communication performance evaluation is the communication rate, which depends on the PRF and the number of symbols in the communication information sequence. If PRF = 30 kHz and $K = 10$, then the corresponding communication transfer rate C is 300 Kbps.

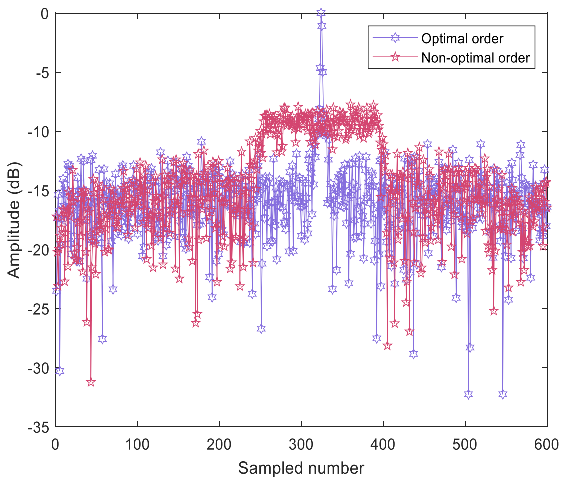

Fig. 10. FRFT of the chirp signal in different orders.

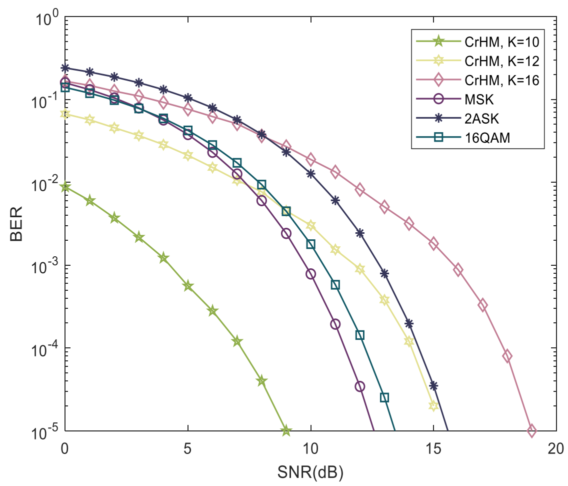

Fig. 11. BER of different signals versus SNR.

5. Conclusion

In this paper, the proposed integrated waveform that can realize radar detection and communication information transmission on a single device simultaneously. The design scheme of the CrHM signal is implemented by a chirp-rate hopping method. The CrHM signal is synthesized through the sub-pulses, which are chirp signals determined by the communication information sequences, and the embedding of communication information is completed by the chirp-rate of each sub-pulse. The CrHM signal has a constant envelope property, and the ambiguity function composed of thumbtack shape and oblique blade shape allows it to achieve high resolution and Doppler tolerance at the same time. Theoretical analysis and simulation results show that the CrHM signal has high performance in the detection of moving target, and the Doppler robustness in communication information demodulation. The multiple bits communication information transmission on single pulse can be realized while ensuring the BER performance.

Acknowledgments

The authors would like to thank the anonymous reviewers and the Associate Editor. This work is supported by the National Nature Science Foundation of China under Grant 62161029, Jiangxi Provincial Natural Science Foundation under Grants 20202BABL202002, 20232BAB212012, SAST2018078.

References

[1] WANG, J., LIANG, X. D., CHEN, L. Y., et al. Waveform designs for joint wireless communication and radar sensing: Pitfalls and opportunities. *IEEE Internet of Things Journal*, 2023, vol. 10, no. 17, p. 15252–15265. DOI: 10.1109/JIOT.2023.3265367

[2] SHI, Q., ZHANG, T. X., YU, X. X., et al. Waveform designs for joint radar-communication systems with OQAM-OFDM. *Signal Processing*, 2022, vol. 195, p. 1–10. DOI: 10.1016/j.sigpro.2022.108462

[3] GAGLIONE, D., CLEMENTE, C., ILIOUDIS, C. V., et al. Fractional Fourier based waveform for a joint radar-communication system. In *IEEE Radar Conference (RadarConf)*. Philadelphia (PA, USA), 2016, p. 1–6. DOI: 10.1109/RADAR.2016.7485314

[4] FENG, Z., FANG, Z., WEI, Z., et al. Joint radar and communication: A survey. *China Communications*, 2020, vol. 17, no. 1, p. 1–27. DOI: 10.23919/JCC.2020.01.001

[5] HAN, Y., EKICI, E., KREMO, H., et al. Spectrum sharing methods for the coexistence of multiple RF systems: a survey. *Ad Hoc Netw*orks, 2016, vol. 53, p. 53–78. DOI: 10.1016/j.adhoc.2016.09.009

[6] ZHOU, S., LIANG, X., YU, Y., et al. Joint radar-communications co-use waveform design using optimized phase perturbation. *IEEE Transactions on Aerospace and Electronic Systems*, 2019, vol. 55, no. 3, p. 1227–1240. DOI: 10.1109/TAES.2019.2909254

[7] LIU, F., MASOUROS, C., PETROPULU, A. P., et al. Joint radar and communication design: Applications, state-of-the-art, and the road ahead. *IEEE Transactions on Communications*, 2020, vol. 68, no. 6, p. 3834–3862. DOI: 10.1109/TCOMM.2020.2973976

[8] ZHOU, Y., ZHOU, H., ZHOU, F., et al. Resource allocation for a wireless powered integrated radar and communication system. *IEEE Wireless Communications Letters*, 2019, vol. 8, no. 1, p. 253–256. DOI: 10.1109/LWC.2018.2868819

[9] CHENG, Z., HE, Z., LIAO, B. Hybrid beamforming for multi-carrier dual-function radar-communication system. *IEEE Transactions on Cognitive Communications and Networking*, 2021, vol. 7, no. 3, p. 1002–1015. DOI: 10.1109/TCCN.2021.3063110

[10] LI, H., LIU, Y., LIAO, G., et al. Joint radar and communications waveform design based on complementary sequence sets. *Remote Sensing*, 2023, vol. 15, no. 3, p. 1–20. DOI: 10.3390/rs15030645

[11] ZHEN, D., ZHANG, Z. H., YU, W. X. A multicarrier phase-coded waveform design scheme for joint radar and communication system. *Chinese Journal. Electronics*, 2021, vol. 30, no. 4, p. 769 to 780. DOI: 10.1049/cje.2021.05.020

[12] QIAN, J., TIAN, F., HUANG, N., et al. Multiobjective optimization for spectral coexistence of radar and communication system. In *IEEE Radar Conference (RadarConf)*. Boston (MA, USA), 2019, p. 1–5. DOI: 10.1109/RADAR.2019.8835742

[13] ZHANG, Q., SUN, H., GAO, X., et al. Time-division ISAC enabled connected automated vehicles cooperation algorithm design and performance evaluation. *IEEE Journal on Selected Areas in Communications*, 2022, vol. 40, no. 7, p. 2206–2218. DOI: 10.1109/JSAC.2022.3155506

[14] RAVENSCROFT, B., MCCORMICK, P. M., BLUNT, S. D., et al. Tandem-hopped OFDM communications in spectral gaps of FM noise radar. In *IEEE Radar Conference (RadarConf)*. Seattle (WA, USA), 2017, p. 1262–1267. DOI: 10.1109/RADAR.2017.7944398

[15] MA, D., SHLEZINGER, N., HUANG, T. Spatial modulation for joint radar-communications systems: Design, analysis, and hardware prototype. *IEEE Transactions on Vehicular Technology*, 2021, vol. 70, no. 3, p. 2283–2298. DOI: 10.1109/TVT.2021.3056408

[16] XU, Z., PETROPULU, A., SUN, S. A joint design of MIMO-OFDM dual-function radar communication system using generalized spatial modulation. In *IEEE Radar Conference (RadarConf20)*. Florence (Italy), 2020, p. 1–6. DOI: 10.1109/RadarConf2043947.2020.9266486

[17] CHEN, X., WANG, X., XU, S., et al. A novel radar waveform compatible with communication. In *International Conference on Computational Problem-Solving (ICCP)*. Chengdu (China), 2011, p. 177–181. DOI: 10.1109/ICCPS.2011.6092272

[18] MA, Q., LU, J., MAOXIANG, Y. Integrated waveform design for 64QAM-LFM radar communication. In *IEEE 5th Advanced Information Technology, Electronic and Automation Control Conference (IAEAC)*. Chongqing (China), 2021, p. 1615–1625. DOI: 10.1109/IAEAC50856.2021.9390784

[19] ZHAO, J., LI, J., YI, Y. Research on radar communication integrated signal based on 64QAM-LFM. In *International Wireless Communications and Mobile Computing (IWCMC)*. Harbin (China), 2021, p. 1151–1155. DOI: 10.1109/IWCMC51323.2021.9498961

[20] GU, Y., ZHAGN, L., ZHOU, Y., et al. Embedding communication symbols into radar waveform with orthogonal FM scheme. *IEEE Sensors Journal*, 2018, vol. 18, no. 21, p. 8709–8719. DOI: 10.1109/JSEN.2018.2868542

[21] GU, Y., ZHANG, L., ZHOU, Y., et al. Waveform design for integrated radar and communication system with orthogonal frequency modulation. *Digital Signal Processing*, 2018, vol. 83, p. 129–138. DOI: 10.1016/j.dsp.2018.08.014

[22] ZHANG, Y., YEH, C., LI, Z., et al. Design and processing method for Doppler-tolerant stepped-frequency waveform using staggered PRF. *Sensors*, 2021, vol. 21, no. 19, p. 1–20. DOI: 10.3390/s21196673

About the Authors ...

Guoqi ZHANG was born in Jiangxi Province, China, in 1999. He received the B.Eng. degree in Electronic Information Engineering from the Pingxiang University, China, in 2022. He is currently pursuing the M.S. degree in Signal Processing from the School of Information Engineering, Nanchang Hangkong University. His current research interests include radar signal processing, radar communication integration and weak target detection.

Xuan RAO was born in Jiangxi Province, P.R. China, in 1977. He received the B.Sc. and M.Sc. degrees from the School of Information Engineering, Nanchang University, Nanchang, China, in 1999 and 2005, respectively; and the Ph.D. degrees from the School of Electronic Engineering, Xidian University, Xi'an, China, in 2015. He is currently an Associate Professor of the School of Information Engineering, Nanchang Hangkong University, China. He is a member of IEEE and his current research interests include radar signal processing, weak target detection and tracking.

Jilin FU was born in Fujian Province, China, in 2000. He received the B.Eng. degree in Electronic Information Engineering from the Qiqihar University, China, in 2023. He is currently pursuing the M.S. degree in Signal Processing from the School of Information Engineering, Nanchang Hangkong University. His current research interests include radar signal processing, radar communication integration and weak target detection.

Wenwen HU received the M.S. degree in Computer Application Technology from the East China Jiaotong University, Nanchang, Jiangxi, China, in 2018, and received the Ph. D. degree in Information System with Shanghai Maritime University, Shanghai, China, in 2022. He now is a lecturer and works in Nanchang Hangkong University. His research interests include the quantum key distribution, quantum secret sharing, quantum and digital images processing.

Jianfen HU (corresponding author) was born in Jiangxi Province, P.R. China, in 1978. She received the Master degree from the School of Measuring and Control Engineering, the Northwestern Polytechnical University, Xi'an, China, in 2005. Her current research interests include signal processing, weak target detection and tracking.